Coexistence of dissociation and annihilation of excitons on charge carriers in organic phosphorescent emitters

J. Kalinowski, W. Stampor, and J. Szmytkowski

Department of Molecular Physics, Gdańsk University of Technology, ul. G. Narutowicza 11/12, 80-952 Gdańsk, Poland

D. Virgili, M. Cocchi, V. Fattori, and C. Sabatini

Institute of Organic Synthesis and Photoreactivity, National Research Council of Italy, via P. Gobetti 101, 40129 Bologna, Italy

We examined exciton quenching mechanisms in organic electrophosphorescent emitters. As an example we have performed detailed steady-state (dc) and alternating (ac) electric-field-modulated (photo)luminescence (EML) studies of the green phosphorescent iridium (III) complex, [Ir$(ppy)_3$], doped into a hole-transporting diamine derivative (TPD) blended with polycarbonate, varying electrode contacts from the hole-injecting indium-tin-oxide (ITO) and Au (dc EML) to the weakly electron-injecting Al on both sides (ac EML) of a sandwich type formed thin film samples. Analysis of ac EML results in terms of the three-dimensional (3D)-Onsager theory of geminate recombination shows that both the EML for the Ir$(ppy)_3$ phosphorescence and TPD fluorescence components of the emission spectrum from the emitters is underlain by the dissociation of Ir$(ppy)_3$ triplet and TPD singlet exciton precursors composed of an electron and a hole separated by a distance $r_0 = 2.1 \pm 0.1$ nm. We find that for samples with the ITO/Au electrode combination, the dissociation is accompanied by exciton annihilation on injected charge. The annihilation proceeds by injected holes with the second order rate constant of $\gamma_{Sq} = (2 \pm 1) \times 10^{-11}$ cm^3/s characterizing the diffusivity of TPD singlets, and $\gamma_{Tq} = (1 \pm 0.5) \times 10^{-14}$ cm^3/s indicative of the relative diffusion motion of the Ir$(ppy)_3$ triplet and a charge carrier. It is shown that the annihilation to dissociation efficiency has a minimum at an electric field of $F_{min} \cong 10^6$ V/cm for the present system but the derived theoretical expression allows us to predict the evolution of F_{min} with various material and sample parameters, and by this to establish criteria to assist in the optimized design of quenching effects in organic electrophosphorescent devices.

PACS number(s): 78.66.Qn, 78.55.Qr, 71.35.−y, 78.60.−b

I. INTRODUCTION

Understanding the mechanisms underlying decay of excited states in solid organic films is one of the most important essentials for the design of highly efficiency electroluminescent emitters in organic light-emitting-devices (LEDs).[1] It is well established that their electroluminescence (EL) quantum efficiency (QE) rolls off at large current densities following the increase in the electric field applied to the devices.[1–10] The high field drop in the QE has been observed in electrofluorescent (EFL)[1,3,7] and electrophosphorescent (EPH)[5,6,8] devices, and found to reduce QE by as much as 0.3 (Refs. 3 and 7) and 0.05 (Ref. 5) of its maximum value, respectively.

There are at least three exciton quenching processes responsible for the high field drop in the QE of organic LEDs: (i) exciton-exciton interaction, (ii) exciton-charge carrier (spin doublet species) interaction, and (iii) exciton dissociation. Both singlet and triplet excitons can be quenched in these processes. Singlet-singlet annihilation has been shown to reduce the photoluminescence (PL) efficiency at high excitation intensity exceeding 10^{21} photons/cm^2 s for a common organometallic complex emitter, tris(8-hydroxyquinoline)aluminum (Alq$_3$), (Refs. 1 and 10) which would correspond to a volume-controlled current density driving the LEDs[1] of $j \cong 100$ A/cm^2. This value exceeds orders of magnitude of the current $j_{max} \cong 50$ mA/cm^2, where the roll-off in the EL QE apparently sets in,[3,10] and seems inaccessible in organic LEDs operated under steady-state

conditions. On the other hand it has been claimed that triplet-triplet annihilation is responsible for the observed decrease in the QE of organic EPH devices.[5,11] The claim has been based on a comparison of the experimental QE-current density (j) plot with the calculated dependence QE(j) resulting from a kinetic analysis of triplet excitons for a red phosphorescent (PH) emitter (PtOEP) embedded in fluorescent (FL) Alq$_3$ dye as a matrix, and an Eu organic chelate-doped in a bipolar conducting host.[5,11] A much worse fit between theory and experiment for PtOEP in other matrices, especially at current densities exceeding 10 mA/cm^2, and failing any one-set parameters fit for the EPH device based on another organic phosphor, the green emitting [Ir$(ppy)_3$] for the chemical names and molecular structures of Ir$(ppy)_3$ see Sec. II], have made the triplet-triplet quenching mechanism questionable or at least insufficient to understand the high field quenching effects in EPH. An attempt to explain the results employing triplet-charge carrier (polaron) annihilation has not been conclusive though its contribution to the quenching effect was not excluded.[5,6] Recent studies of excitonic interactions in PtOEP,[12] and Ir$(ppy)_3$,[13] doped layers and their neat solid thin films have shown the current density threshold for the QE reduction by triplet-triplet interaction quenching to be on the order $(0.5–1)$ A/cm^2, exceeding largely experimental values falling in the tens of mA/cm^2 range.[12,13] The electric field (F)-enhanced exciton dissociation seemed an alternative for the high-field decrease in the QE of organic LEDs. Indeed, an analysis based on the Poole-Frenkel (PF) charge separation mechanism led to a good agreement to the

curvature of the decreasing part of the QE(F) function for Alq₃-based EF LEDs, but the extracted characteristic PF parameter appeared approximately a factor of 2 smaller than its theoretical value.[14] Therefore, microscopic conditions of the exciton dissociation process had to be specified, e.g., local temperature, or another model for exciton dissociation proposed. In our recent works we have demonstrated that the three-dimensional (3D) Onsager theory of geminate recombination[15] can be successfully applied to explain the photodissociation of singlet excitons in solid films of Alq₃[16] and the high field roll-off in the QE of organic EL devices based on the PH molecule Ir$(ppy)_3$.[6] However, comparing the high-field imposed QE reduction from the EPH device with PL quenching by an external electric field applied to neat Ir$(ppy)_3$ films, one arrives at the conclusion that the field separation of the carriers depends on the production mechanism of the emissive states. This would reflect in the type of charge pairs preceding the dissociation events and could alter the interrelation between various quenching mechanisms of the excited states. For instance, the average intercarrier distance of charge pair precursors of the excitons appears to differ largely in neat ($\geqslant 3.5$ nm) and blend (≈ 2 nm) Ir$(ppy)_3$ films.

We are concerned in this work with low optical excitation ($<10^{15}$ photons/cm² s) of thin film amorphous emitters, where a phosphorescent guest molecules are dispersed within a conductive host matrix made of a hole transporting material blended with a polymer. Proceeding from optical exciton formation, we study the dynamics of singlets and triplets of optically active molecules under steady-state conditions until the point of their radiative or nonradiative decay. Such films subjected to an electric field can be considered as a model for the emission layer in EPH LEDs, though the excitation mode is different. The low-intensity optical excitation conditions allow us to examine the exciton quenching mechanisms ignoring exciton-exciton interactions. Varying the electrode material and its electrical bias we were able to separate the coexisting exciton dissociation and exciton-charge carrier annihilation processes, thus to find their relative contributions as a function of applied field and various emitter parameters. We conclude by summarizing the types of singlet and triplet reactions in PH emitters in electric fields applied with ohmic and weakly-injecting electrodes, and showing methods for minimizing nonradiative exciton losses.

The paper is organized in five sections. In Sec. II the experimental procedures are described, including the presentation of the materials used. Section III presents the measured relative PL efficiency in steady-state (dc) and alternating (ac) electric fields applied through different material and polarization combinations of electrodes to several organic phosphor-doped solid films. The results are discussed in terms of exciton dissociation and annihilation by injected charge in Sec. IV. Conclusions are presented in Sec. V.

II. EXPERIMENTAL TECHNIQUES

ac and dc electromodulation of luminescence (EML) and dc photoconduction (PhC) measurements were performed
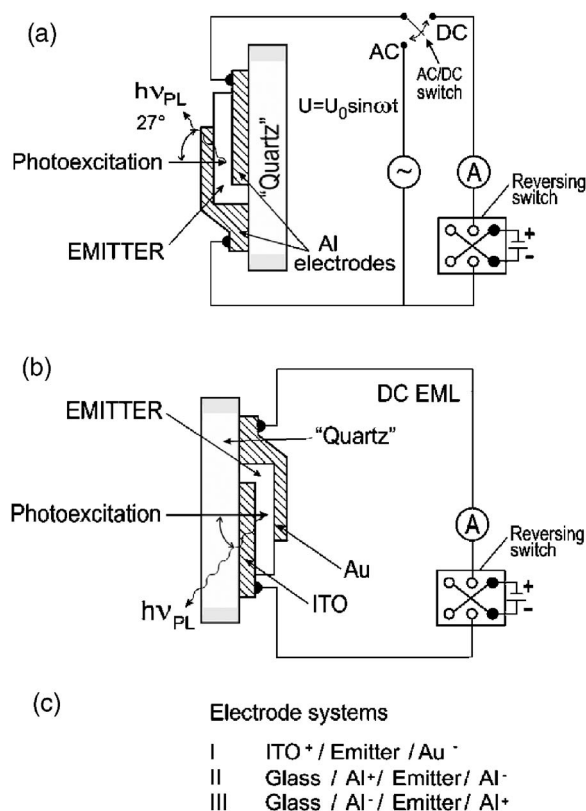

FIG. 1. The experimental setup of the ac and dc electromodulation (EML) of the photoluminescence (PL) efficiency and dc photoconduction (PhC) in thin films of phosphorescent (PH) emitters. PL from the optically excited emitter is measured from the front-face of the sample with the detection angle 27° (chosen arbitrarily) in order to avoid detection of the reflected part of the exciting light. The dc EML and PhC measurements can be conducted illuminating the sample through either a positively or negatively biased non-substrate (top) electrical contact of Al (a) or substrate deposited ITO (b) using the reversing switch. (c) Electrode systems and electrode polarization combinations used.

on doped-blend film emitters of Ir$(ppy)_3$ prepared by spin coating.

A. Preparation of the samples

To compare the exciton quenching in the presence and in the absence of space charge in organic PH emitters, different combinations of electrodes have been used and electric field applied to optically excited thin organic films as shown in Fig. 1. The sandwich type samples were fabricated on cleaned glass (or quartz) substrates precoated with indium-tin-oxide (ITO) with a sheet resistance of $\cong 20$ Ω/sq or a semitransparent film of Al. All phosphor-doped emitter layers (Fig. 2) were prepared by spin coating from a 10 mg/ml dichloromethane solution. Chosen spin coating conditions (2000 rpm) led to a 50–150 nm thick emitter films which after drying were covered by a vacuum-evaporated top semitransparent top electrode of gold or aluminum. The active electrode areas were between 0.05 and 0.2 cm². The materials used are: [Ir$(ppy)_3$] fac tris(2-phenyl-
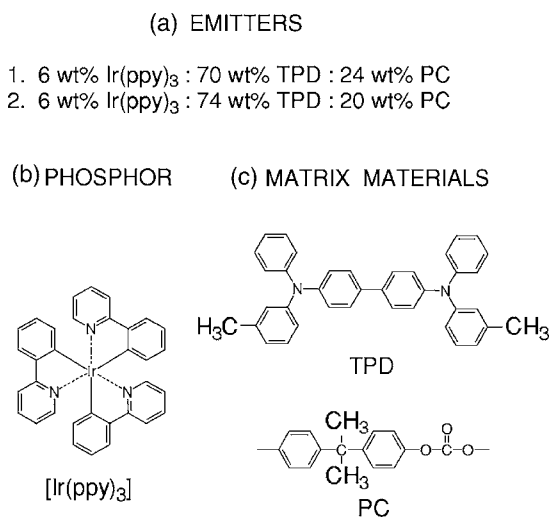
(a) EMITTERS

1. 6 wt% Ir(ppy)$_3$: 70 wt% TPD : 24 wt% PC
2. 6 wt% Ir(ppy)$_3$: 74 wt% TPD : 20 wt% PC

(b) PHOSPHOR   (c) MATRIX MATERIALS

TPD

[Ir(ppy)$_3$]

PC

FIG. 2. The emitters used to observe the EML and PhC (a), Ir(ppy)$_3$ organic phosphor (b) incorporated in solid state films of blended TPD and PC (c). For chemical names of the molecules see text.

pyridine), TPD (N,N'-diphenyl-N,N'-bis(3-methylphenyl)-[1,1'-biphenyl]-4,4'-diamine, and PC (bisphenol-A-A-polycarbonate). Of these materials, TPD is predominantly a hole transporting material and PC is electronically inert. The phosphor, [Ir(ppy)$_3$], is employed as a guest molecule emitting PH light at ~510 nm[6] being redshifted with respect to the FL emission of TPD occurring at ~420 nm[1,17] (see also Sec. III A).

B. Electromodulation measurements

The luminescence of the emitters listed in Fig. 2(a) was excited by a light beam directed parallel to the steady state (dc) or alternating (ac) field direction. The modulation of photoluminescence (PL) by an ac electric field was detected by a photomultiplier tube placed in front of the sample in a position allowing the reflected exciting light to be effectively avoided [Fig. 1(a)]. Electromodulation of the luminescence (EML) was induced by a sinusoidal field [$F(t)=F_0 \sin(\omega t)$] with $\omega/2\pi$ between 200 Hz and 2 kHz. The electrical signal derived from the photomultiplier consisted of a steady-state and alternating components corresponding to the time-dependent luminescence signal expanded in a Fourier series $I(t)=\Sigma I_{n,\omega}(t)$ ($n=0,1,2,\ldots$). The quantity to be monitored as a function of electric field and excitation wavelength is defined here as

$$(2\omega)\mathrm{EML} = \frac{I_{2\omega}(F)}{I_{0\omega}(F)}, \quad (1)$$

where $I_{0\omega}$ and $I_{2\omega}$ are the zeroth, and second Fourier components of the luminescence intensity in the presence of an ac modulating field with amplitude F_0. A more detailed description of the ac EML measurements is given elsewhere.[18] If $I_{2\omega}(F)$ can be approximated by a second order power function of the rms field, $F_{\mathrm{rms}}=F_0/\sqrt{2}$, the ac ($2\omega$) EML signal translates in a PL intensity change [$I(0)-I(F_0)]/I(0)$
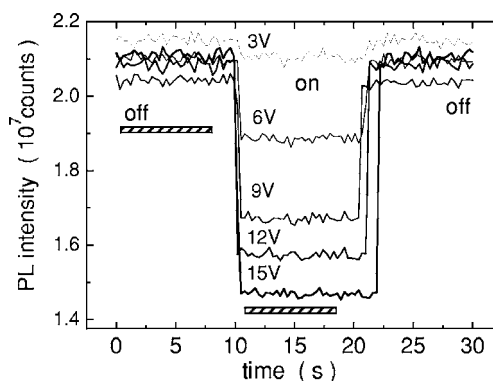

FIG. 3. Illustration of the PL intensity response of an ITO$^+$/emitter/Au$^-$ structure to the varying dc voltage as described in the left bottom corner of the transients. The field dependent reduction of the PL intensity is seen, the initial PL level being restored after switching off the voltage 10 s after its switching on.

$=\sqrt{2}I_{2\omega}(F_{\mathrm{rms}})/I_{0\omega}(F_{\mathrm{rms}})$ describing simply the dc PL quenching imposed by a steady state field of $F=F_0$. The PL quenching ratio as a function of the steady-state applied field [Fig. 1(b)] was obtained by applying a progressively increasing dc voltage and taking an average PL intensity over a time of about 10 s before (Φ_0) and after (Φ) the voltage rise step for each value of the voltage, an example is shown in Fig. 3. The PL intensity was sampled every 0.3 s with a Spex Fluorolog 2 spectrofluorimeter, the results displayed by the ratio

$$\delta(F) = \frac{|\Phi(F) - \Phi_0|}{\Phi_0} = \frac{|\Delta\Phi(F)|}{\Phi_0}, \quad (2a)$$

or

$$\delta'(F) = \frac{|\Phi(F) - \Phi_0|}{\Phi(F)} = \frac{|\Delta\Phi(F)|}{\Phi(F)}, \quad (2b)$$

as a function of the electric field (F) within the emission ranges corresponding to the PH of the dopant and FL of the hole transporting material, TPD. For $|\Delta\Phi(F)| \ll \Phi(F)$, $\delta'(F) \cong \delta(F)$. All dc electric field-induced PL modulation measurements were carried out on the samples held in the argon atmosphere. To observe the weak FL component of the total emission spectrum of the emitter in ac modulation experiments, a BG12, GG400 glass filters and an interference filter (425 nm) have been applied to remove the PH emission band. The excitation level did not exceed 10^{13} quanta/cm^2 s at the excitation wavelengths used, $\lambda_{\mathrm{exc}}=350$, 366, or 436 nm.

C. Conduction and photoconduction

The steady-state electrical conduction and photoconduction (PhC) measurements were performed with emitter 1 for electrode systems I to III [see Figs. 1 and 2]. The term "emitter" is used here to identify the layer containing emissive molecular species (molecular emitters), but not molecular emitters themselves. A Narva 200 W mercury lamp and an Osram 150 W xenon lamp were used as light sources. The photocurrent was measured within the quantal intensity
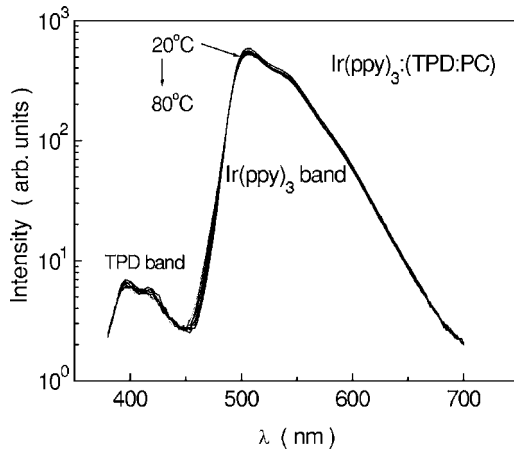
FIG. 4. The emission spectra of (60–70 nm) thick emitters (2), recorded at seven different temperature varied by a 10 °C step from 20 to 80 °C. The TPD FL band at about 420 nm is almost two orders of magnitude weaker than the Ir$(ppy)_3$ PH band peaking at about 510 nm.

range $10^{12} < I_{exc} < 10^{15}$ quanta/cm^2 s and dc field range between 3×10^3 and 5×10^5 V/cm.

III. EXPERIMENTAL RESULTS

In this section EML, PhC, and dark dc electrical conduction results obtained on emitters specified in Sec. II (cf. Fig. 2) are reported. In Sec. III A we demonstrate the existence of exciton dissociation effects in the systems studied. Then in Sec. III B we examine the EML in the presence of injected charge. We find the enhanced quenching efficiency to be a result of the coexistence of dissociation and annihilation of singlet (S-q) and triplet (T-q) excitons by charge carriers. We found the dissociation component to be well described by the 3D Onsager theory of geminate recombination[15] and the annihilation component to follow a simple kinetic model for S-q and T-q exciton quenching by charge carriers (holes).

A. Electromodulated PL efficiency

EML experiments were performed on the PH emission peaking at $\cong 510$ nm, characteristic of Ir$(ppy)_3$, and FL of TPD, peaking at $\cong 420$ nm. The overall PL spectrum of an Ir$(ppy)_3$-doped (TPD:PC) sample at various temperatures is displayed in Fig. 4. Figure 5 shows the measured electromodulated signals δ (2a) of the relative PL efficiency as a function of the electric field strength applied to two different samples of emitter (1) taken from an eight sample bench obtained under one preparation cycle, and to one sample of emitter (2) using electrode system II (see Fig. 1). The data for a stronger-doped [10 wt. % Ir$(ppy)_3$] sample are added for comparison. Because of relatively low modulation signals (<2%) the modulation ratio δ (2a) could be here identified with δ' (2b). The experimental ac-dc converted data (points) are compared with theoretical predictions of the 3D-Onsager recombination model (solid lines), assuming the exciton dissociation to be the only pathway of the field-induced nonradiative decay of photoexcited states (cf. Sec. IV). The
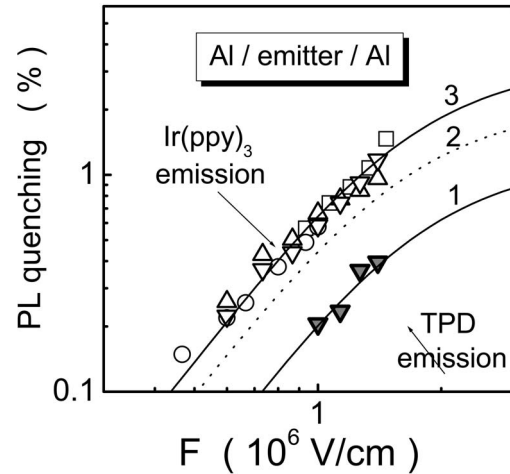

FIG. 5. PL quenching (δ) as a function of dc electric field applied to four emitters with electrode system II (the rms values of the ac field strength are converted to their dc equivalents $F = F_0/\sqrt{2}$; cf. Sec. II B): emitter 1, two samples taken from a set of a sample bench obtained under one preparation cycle (triangles); emitter 2, one sample (circles); squares show results obtained for an emitter containing 10 wt% of Ir$(ppy)_3$. Two of the three plots represent the data for the FL emission of the host component TPD (plot 1) and PH emission from the phosphor dopant (plot 3). All samples excited at $\lambda_{exc} = 366$ nm. The solid curves are Onsager fits to the data using Eq. (14) and demonstrate good agreement with behavior expected for exciton dissociation. The dotted line (plot 2) represents the PL quenching due solely to the dissociation of Ir$(ppy)_3$ triplets, and is extracted from the data of plot 3 accounted for quenching of TPD singlets given by plot 1. The best fit to the data is obtained with the following Onsager model parameters: $\eta_0 = 0.014$, $r_0 = 2.1$ nm for plot 1, $\eta_0 = 0.025$, $r_0 = 2.2$ nm for plot 2. The initial electron-hole separation distance, r_0, has been calculated from the fitting parameter r_0/r_c taking the Onsager radius $r \approx 19$ nm typical for organic materials ($\varepsilon = 3$) at room temperature.

nominal, $F_0 = U/d$, electric field has been used throughout the analysis since the internal field, $F_i \approx 10^4$ V/cm, due to the photogenerated charge, was too weak to affect the field noticeably. The F_i was determined from the proportionality of the modulation signals at the first, 1ω (EA), and second, 2ω (EA), harmonic of the electroabsorption (EA) signals as described in Ref. 19. In Fig. 6, the [Ir$(ppy)_3$] and TPD emission quenching data for electrode system I are compared with those for systems II and III. For the electrode configuration ITO(+)/Au(−) (system I) the field effect on the PH exceeds up to four times that on the FL of TPD. The Onsager fits from Fig. 5, representing the dissociation efficiency $\delta_{dis} = [(\Phi_0 - \Phi)/\Phi_0] = \Delta\Phi/\Phi_0$, are compared with those obtained with the same emitter but different material and configurations of electrodes in Fig. 7. They are displayed by selected points along with dc quenching data (δ) for electrode system II and the charge quenching component, $\delta_q = \delta - \delta_{dis}$ (see Sec. IV).

B. Electric and photoelectric characteristics

The electrical behavior of emitters studied differs depending on the electrode configuration. No photoconduction is
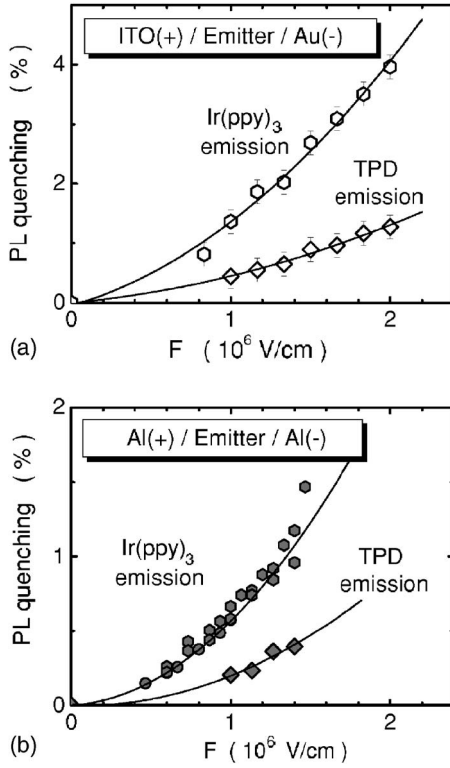
FIG. 6. The electric field dependence of the PH Ir(ppy)$_3$ and FL TPD components of the PL quenching in emitter 1 using electrode system I (a) and II (b). The solid lines are guides to the eyes.

observed for the ITO/Au configuration [system I in Fig. 1(c)]. Thus, its electrical conduction is determined by the thermionic hole injection from the ITO anode. Assuming the EML effect to be enhanced substantially by the injected charge, one would expect the ITO(+) anode to be an ohmic contact producing a space-charge-limited current (SCLC) which in the case of the Poole-Frenkel type field dependent mobility can be expressed as[20,21]

$$j_{SCLC} \cong \frac{9}{8} \frac{\varepsilon_0 \varepsilon \mu_0 F^2}{d} \exp(0.891\beta_\mu F^{1/2}), \qquad (3)$$

where d is the emitter thickness.

Indeed, the current-voltage characteristic in this case is well approximated by a straight-line $\ln(j/F^2) - F^{1/2}$ plot suggesting the current to be a SCLC with the field dependent mobility, $\mu_{eff} = \mu_0 \exp(\beta_\mu F^{1/2})$, where μ_0 is the zero-field mobility and $\beta_\mu \cong 4 \times 10^{-3}$ (cm/V)$^{1/2}$ is the scaling factor similar to that resulted from time-of-flight measurements of hole mobility in TPD-doped PC organic films[22,23] [see Fig. 8(a)]. We do not analyze the reverse polarization currents because they are largely deformed by the nature of the vacuum-evaporated Au$^+$ injection contact. It is known that applying a high electric field to metal-insulator-metal structures introduces electrode material into dielectric, forming metallic inclusions. For example, a field-induced Au$^+$ ion diffusion from Au anode into C$_{70}$ films has been invoked to explain 2 to 3 orders of magnitude increase of their electrical conductivity with the field application time.[24] The additional
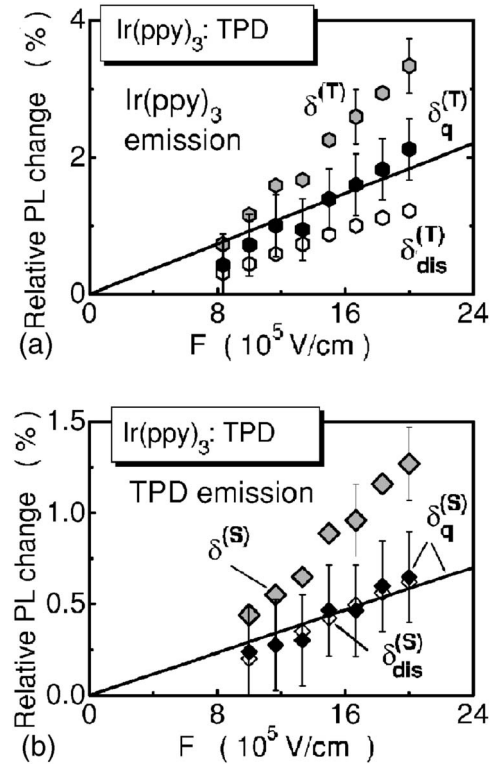

FIG. 7. The dependence of the dissociation (δ_{dis}) and charge-induced (δ_q) components of the overall (δ) PL quenching on the applied electric field for Ir(ppy)$_3$ triplets [$\delta^{(T)}$] and TPD singlets [$\delta^{(S)}$] in Ir(ppy)$_3$-doped (TPD:PC) blend (a 120 nm-thick emitter 1). The charge quenching component is determined by the difference between the overall effect with the electrode system I and system II, $\delta_q = \delta - \delta_{dis}$. The solid straight lines are predictions of PL quenching by the space charge of holes injected from the ITO(+) anode. From the slopes of the straight lines the second order rate constants $\gamma_{Sq} = (2 \pm 1) \times 10^{-11}$ cm^3/s for hole—TPD singlet exciton and $\gamma_{Tq} = (1 \pm 0.5) \times 10^{-14}$ cm^3/s for hole-Ir(ppy)$_3$ triplet exciton interaction are calculated using $\varepsilon = 3$ at room temperature.

current is thus supposed to occur due to tunneling between metallic inclusions (see an overview in Ref. 25), the current, though strongly field dependent, is no longer SCLC. The effect is absent with the initial ITO$^+$ bias, and becomes largely reduced (or negligible) on changing Au$^+$ to ITO$^+$ bias since the fine net of Au inclusions is reformed and bulk conductivity of the sample reestablished.

Weak photocurrents (i_{ph}) occur under illumination within the spectral range 300−500 nm for the configuration Al/Al [Fig. 8(b)].

IV. ANALYSIS AND DISCUSSION OF RESULTS

A. Kinetic model for excitonic processes

To understand the EML results described in Sec. III A, we generalize a kinetic model for excitonic processes to include the electric field dependence of microscopic rate constants for decay of primary and relaxed molecular excitonic states. An energy level diagram for the kinetics of exciton formation and decay in the presence of electric field is shown in
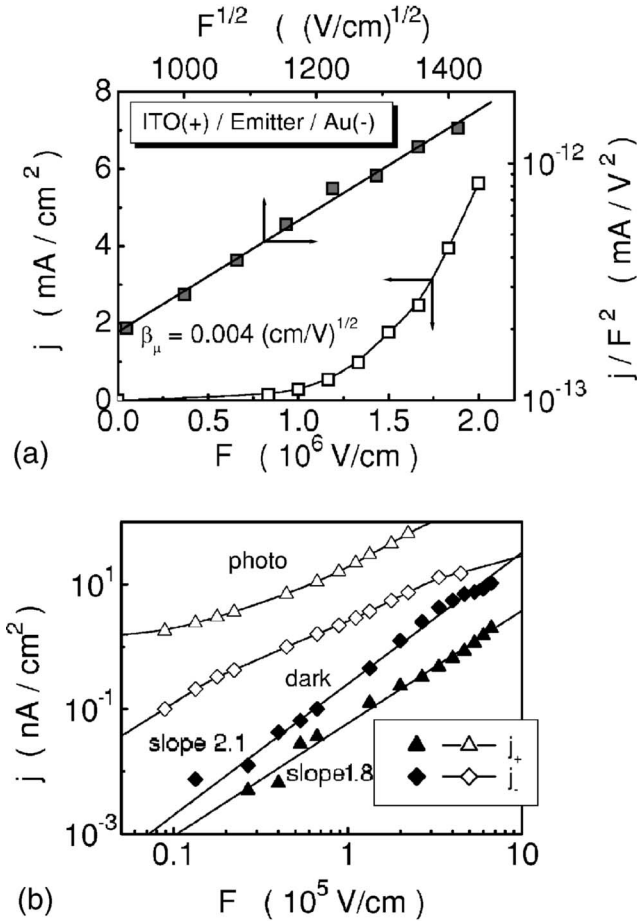
FIG. 8. (a) The current density (j)—electric field (F) dependence for emitter 2 ($d=60$ nm) with the electrode combination ITO($+$)/Au($-$) in the linear (open figures) and $\ln(j/F^2)$ vs $F^{1/2}$ (full figures) representations. The straight-line plot of the latter indicates the structure to be driven by SCLC conditions with a Poole-Frenkel-type field-dependent mobility. (b) The dark-current and photocurrent (photo) field characteristics for a 150 nm thick blend emitter 1 for the positive (j_+) and negative (j_-) bias of the illuminated top electrode of Al electrode system II. The photocurrents are excited with the light of $\lambda_{\text{exc}}=366$ nm at an intensity of $I=10^{13}$ ph/cm^2 s.

Fig. 9. Here $\alpha I_0[1-\eta_X^{(S)}]$ is the rate of creation of host singlet excitons (S_X), α is the linear absorption coefficient of the exciting light ($h\nu_{\text{exc}}$) of intensity I_0, $\eta_X^{(S)}$ is the dissociation efficiency of S_X singlets; $k_X^{(\text{ISC})}$ is the rate constant for the intersystem crossing of singlets to triplets (T_X), the process competing with the monomolecular decay of S_X to the ground state S_0 and quantified by the overall rate constant $k_X^{(S)}$ which includes the component of the radiative decay underlying the host FL ($h\nu_{\text{FL}}$); $k_{XY}^{(S)}$ is the rate of Förster energy transfer to the guest molecules Ir(ppy)$_3$; $\eta_Y^{(S)}$ and $\eta_Y^{(T)}$ are the dissociation efficiencies of guest singlets (S_Y) and triplets (T_Y), respectively; $k_Y^{(\text{ISC})}$ is the rate constant of the intersystem crossing $S_Y \to T_Y$. The monomolecular decay rate constant $k_Y^{(S)}$ is negligible due to the highly efficient intersystem crossing process [large $k_Y^{(\text{ISC})}$]. The PH emission ($h\nu_{\text{PH}}$) of the guest Ir(ppy)$_3$ is driven by the radiative component of
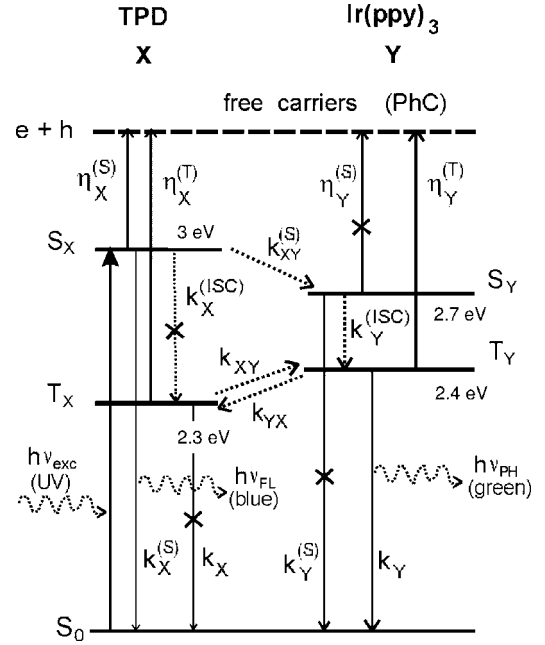

FIG. 9. Energy levels and some photophysical processes in the Ir(ppy)$_3$:TPD:PC system. The ground state level has been chosen as a reference level (i.e., $E=0$). The excitation photons ($\lambda_{\text{exc}}=350$ nm), harvested by concentration dominating TPD (X) molecules, form singlet TPD excitons (S_x). Their radiative decay produces the TPD blue FL ($h\nu_{\text{FL}}$), the intersystem crossing ($k_X^{(\text{ISC})}$) to triplets as well as the monomolecular triplet decay (k_X) are negligibly small as compared with the rapid energy transfer ($k_{XY}^{(S)}$) to guest phosphor molecules, Ir(ppy)$_3$ (Y), their excited singlets (S_Y) intercrossing to triplet states (T_Y) produce green PH light ($h\nu_{\text{PH}}$). Of four dissociation channels, the dissociation of S_Y singlets can be neglected since their intersystem crossing, $k_Y^{(\text{ISC})}$, to T_Y appears to be much more efficient. Processes ineffective in exciton decay are marked with a cross. The monomolecular decay rate constants $k_X^{(S)}$ and k_Y, and dissociation efficiencies $\eta_X^{(S)}$, $\eta_X^{(T)}$, and $\eta_Y^{(T)}$ are subject to the electric field modulation.

the monomolecular decay rate k_Y. The rates of forward (k_{XY}) and back (k_{YX}) Dexter energy transfer between T_X and T_Y have been shown to participate in establishing an equilibrium with $k_{YX}/k_{XY}=T_X/T_Y$.[26]

To infer on the electric field-imposed exciton quenching it is necessary to obtain expressions for the host (TPD) FL and guest [Ir(ppy)$_3$] PH intensities as a function of the electric field. These intensities are proportional to the populations of the relaxed excited states, S_X and T_Y, respectively, and the steady-state kinetic equations describing these populations are

$$\dot{S}_X = \alpha I_0 - k_{Xtot}^{(S)} S_X = 0, \tag{4}$$

$$\dot{S}_Y = k_{XY}^{(S)} S_X - k_Y^{(\text{ISC})} S_Y - k_Y^{(S)} S_Y = 0, \tag{5}$$

$$\dot{T}_X = k_X^{(\text{ISC})} S_X + k_{YX} T_Y - (k_{XY} + k_X) T_X = 0, \tag{6}$$

$$\dot{T}_Y = k_Y^{(\mathrm{ISC})} S_Y + k_{XY} T_X - (k_{YX} + k_Y) T_Y = 0, \quad (7)$$

where $k_{Xtot}^{(S)} = k_X^{(S)} + k_X^{(\mathrm{ISC})} + k_{XY}^{(S)}$.

These equations are readily solved if we consider the case with the following inequalities to be fulfilled: $k_X \ll k_{XY}$, $k_Y \ll k_{YX}$, $k_X^{(\mathrm{ISC})} \ll k_X^{(S)}$, $k_Y^{(S)} \ll k_Y^{(\mathrm{ISC})}$, and $k_X \ll k_Y$ as proved for the present system, Ir$(ppy)_3$:TPD:PC, by the time-dependent PH study varying the relative concentration of the phosphor, Ir$(ppy)_3$.[26] The field dependence of both S_X and T_Y occurs through the field-dependent monomolecular decay rate constants $k_X^{(S)}$ and k_Y. In general, they increase with electric field due to both the relaxed field-assisted exciton dissociation into electron-hole pairs and interaction with field-increasing concentration of the charge injected at electrical contacts (see Sec. IV C). However, unlike the dissociation of near absorption edge excited states in conjugated polymers,[27] the dissociation of relaxed excited states in low-molecular weight organic dyes does not show up in the field-dependent rate quenching mechanism.[28,29] Therefore, we assume the electric field effect on dissociation to appear on the initially excited (nonrelaxed) host singlet $[\eta_X^{(S)}]$ and guest triplet $[\eta_Y^{(T)}]$ precursors of the final emissive states, the effect to be observed through the amplitude quenching of the time-resolved luminescence. Then, the concentrations of host singlets and guest triplets resulting from the solutions of Eqs. (4)–(7) must be multiplied by suitable field-dependent reduction factors $[1 - \eta_X^{(S)}]$ and $[1 - \eta_Y^{(T)}]$. We obtain

$$S_X(F) = \frac{\alpha I_0 [1 - \eta_X^{(S)}(F)]}{k_{Xtot}^{(S)}(F)}, \quad (8)$$

$$T_Y(F) = [1 - \eta_Y^{(T)}(F)] \frac{\alpha I_0 [1 - \eta_X^{(S)}(F)]}{k_{Xtot}^{(S)}(F)} \frac{k_{XY}^{(S)}}{k_{Ytot}(F)}, \quad (9)$$

where $k_{Ytot}(F) = k_{YX} + k_Y(F)$ with $k_Y(F) = k_Y(0) + k_q^{(T)}(F)$. The $k_q^{(T)}$ represents the guest triplet decay component due to triplet-charge carrier interaction, thus being a function of the applied field. Since $\Phi_X^{(S)}(F) \sim S_X(F)$, $\Phi_X^{(S)}(0) \sim S_X(0)$, and $\Phi_Y^{(T)}(F) \sim T_Y(F)$, $\Phi_Y^{(T)}(0) \sim T_Y(0)$, the overall field-induced PL quenching ratio (2b) can be approximated by

$$\delta' \cong \delta^{(T)\prime} + \delta^{(S)\prime} = [\delta_q^{(T)\prime} + \delta_{dis}^{(T)}] + [\delta_q^{(S)\prime} + \delta_{dis}^{(S)}] \quad (10)$$

using the zero-field FL and PH intensities $\Phi_X^{(S)}(0)$ and $\Phi_Y^{(T)}(0)$ determined from Eqs. (8) and (9) with $\eta_X^{(S)} = \eta_Y^{(T)} = 0$ and constant values of $k_{Xtot}^{(S)}(0)$ and $k_{Ytot}(0)$. Equation (10) has been derived with reasonable assumptions $\eta_X^{(S)}$, $\eta_Y^{(T)} \ll 1$ and moderate values of $\delta_q^{(S)\prime}$, $\delta_q^{(T)\prime}$. Experimentally, $\delta^{(S)\prime}$ and $\delta^{(T)\prime}$ can be separated by measuring EML on the host and guest emission bands apparent in the PL spectrum of Fig. 4. Given that $\delta_{dis}^{(S)\prime} = \delta_{dis}^{(S)}$ and $\delta_{dis}^{(T)\prime} = \delta_{dis}^{(T)}$ are measured with the Al/emitter/Al structure (Fig. 5), it is possible to extract $\delta^{(S)\prime} = \delta^{(S)\prime} - \delta_q^{(S)}$ for the emission of TPD and $\delta^{(T)\prime} = \delta^{(T)\prime} - \delta_{dis}^{(T)}$ for the emission of Ir$(ppy)_3$ when the ITO/Au electrode combination is used (Fig. 6). The results are displayed in Fig. 7 comparing the total quenching, δ, with its dissociation, δ_{dis}, and charge-induced, δ_q, components for both the FL of TPD and PH of Ir$(ppy)_3$. We note that the field dependence of $\delta_{dis}^{(T)}$

displayed in Fig. 7(a) is based on the data of Fig. 5 represented by curve 2 correcting the measured effect on the PH (curve 3) for the EML of TPD (curve 1).

B. Exciton dissociation

According to the analysis of Secs. IV A and IV D, the EML observed with emitters sandwiched between two Al electrodes is due to the electric-field assisted dissociation of host singlet (S_X) and triplet (T_X), and guest triplet (T_Y) excitons. The exciton dissociation is commonly considered as a two-step process: (i) the initial separation (r_0) forming a two-particle system of geminate electron (e)-hole (h) pair (e-h), and (ii) the diffusive motion in their mutual Coulomb field.

The probability $[\eta(r)]$ that a pair with an e-h separation distance r escapes geminate recombination can be calculated by solving the differential equation[30]

$$D\left[\nabla^2 \eta(r) - \frac{1}{kT} \nabla \varphi(r) \nabla \eta(r) \right] - K(r) \eta(r) = 0, \quad (11)$$

where D is the sum of the diffusion coefficients of the charge carriers and $\varphi(r)$ is their potential energy, which in the presence of an external electric field (F) directed along r is given by

$$\varphi(r) = -\frac{e^2}{4\pi \varepsilon_0 \varepsilon r} - eFr. \quad (12)$$

Here, e stands for the electronic charge, ε_0 is the vacuum dielectric permittivity, ε is the relative dielectric constant, k is the Boltzmann constant, and T is the temperature. The crucial point is the reaction rate constant $K(r)$ determining the sink term $-K(r)\eta(r)$. This constant is a function of r reflecting boundary conditions for Eq. (11). Even a relatively simple exponential function $K(r) = A \exp[-c(r-L)]$ with a scaling parameter c and $A = K(r)$ at the charge contact distance $r = L$, requires advanced numerical methods to solve Eq. (11). However, the calculations made with such a distance-dependent intrinsic reaction rate and $L = 0.6$ nm show $\eta(F)$ to be well approximated by the 3D Onsager model[16] for a steep functions of $K(r)$ (e.g., $c = 0.1$ nm^{-1}).[31] This model assumes the recombination probability equal 1 to occur at $L = 0$. In the absence of external electric field the escape probability is given by

$$\eta(r_0, F = 0) = \exp(-r_c/r_0), \quad (13)$$

where r_c is the Onsager radius defined by $r_c = e^2/4\pi \varepsilon_0 \varepsilon kT$, and r_0 is the initial e-h separation distance. In the presence of an external field, the escape probability averaged over the charge pair orientation increases according to [15,32]

$$\eta(r_0, F) = \eta_0 \left[1 - \xi^{-1} \sum_{m=1}^{\infty} P_m(r_c/r_0) P_m(\xi) \right], \quad (14)$$

where η_0 defines the initial field-independent dissociation efficiency, $P_m(\xi)$ is the incomplete γ function of integral order m, and $\xi = e r_0 |F|/kT$. We fit the field dependence of the EML from Al/emitter/Al structures to Eq. (14) to determine the values of η_0 and r_0. The fits are accurate for electric fields

above 0.5×10^6 V/cm proving the Onsager model 1938 can be successfully used to predict the EML in the absence of space charge (see Fig. 5).

C. Charge modulation of PL

An additional quenching mechanism appears in emitters containing space charge. This is the exciton-charge carrier annihilation process expected to operate with our ITO(+)/emitter/Au(−) structure (see Sec. III A). As discussed previously, the j-F dependence observed in this structure reveals the SCLC features with discrete traps and field-dependent mobility. It therefore follows that the average concentration of charge (holes) in the bulk of the emitter is proportional to the applied field:[1,33]

$$\bar{n} = \frac{3}{2}\frac{\varepsilon_0 \varepsilon}{e}\frac{F}{d}, \qquad (15)$$

where d is the emitter thickness.

The charge interaction with excitons increases the monomolecular rate constants for both singlet and triplet excitons by terms $\gamma_{Sq}\bar{n}$ and $\gamma_{Tq}\bar{n}$, where γ_{Sq} and γ_{Tq} are the second order rate constants for singlet exciton- and triplet exciton-charge carrier interaction, respectively. One would expect the charge quenching components of the EML signal

$$\delta_q^{(S)} = \frac{3}{2}\frac{\varepsilon_0 \varepsilon}{ed}\tau_S \gamma_{Sq} F \quad \text{and} \quad \delta_q^{(T)} = \frac{3}{2}\frac{\varepsilon_0 \varepsilon}{ed}\tau_T \gamma_{Tq} F \qquad (16)$$

to be proportional to the applied field assuming the intrinsic lifetime and the interaction rate constants of excitons, $\tau_S = [k_{tot}^{(S)}(F=0)]^{-1}$ and γ_{Sq} for singlets, and $\tau_T = [k_{tot}^{(T)}(F=0)]^{-1}$ and γ_{Tq} for triplets, to be field independent. Both $\delta_q^{(S)}$ and $\delta_q^{(T)}$ can be fairly well approximated by straight-line plots as shown in Fig. 7. From their slopes $\gamma_{Sq} = (2 \pm 1) \times 10^{-11}$ cm^3/s and $\gamma_{Tq} = (1 \pm 0.5) \times 10^{-14}$ cm^3/s follow using $\varepsilon = 3$, $d = 150$ nm, $\tau_S = 1$ ns[34] and $\tau_T = 7$ μs.[26] If the quenching process is governed by the relative motion of the exciton and the carrier (hole), the sum of their diffusion coefficients can be calculated on the basis of these values of $\gamma_{S,Tq}$

$$D_{S,T} + D_q = \gamma_{S,Tq}/4\pi R, \qquad (17)$$

where $D_{S,T}$ and D_q are the diffusion coefficients of the singlet or triplet exciton and the carrier, respectively, and R is the exciton capture radius. The Einstein relation correlates directly D_q with the carrier mobility μ, $D_q = \mu kT/e$. Therefore, in disordered solids with a field dependent mobility (see Sec. III B), one would expect $\gamma_{S,Tq}$ to vary with electric field. The approximately linear increase of the emission quenching with field (Fig. 7) indicates, however, $D_{S,T} \gg D_q$ and $\gamma_{S,Tq}$ to be constants determined by the motion of singlet and triplet excitons with the respective diffusion coefficients $D_S \cong 3 \times 10^{-5}$ cm^2/s and $D_T = 8 \times 10^{-9}$ cm^2/s obtained from Eq. (17) with a reasonable assumption $R \cong 1$–2 nm identified either with an average spacing between molecules of TPD or Ir(ppy)$_3$. The value of D_S is two orders of magnitude smaller than that found in neat TPD films.[34] The obvious reason for

this difference is the strongly competitive process of singlet energy transfer to Ir(ppy)$_3$ molecules in Ir(ppy)$_3$-doped (TPD:PC) blend films studied in the present work (see Fig. 9). Let us consider a sample of 6% Ir(ppy)$_3$: 75% TPD : 19% PC in which the average intermolecular distance of TPD host molecules is $R_{XX} \cong 0.98$ nm and average host-guest intermolecular spacing $R_{XY} \cong 0.85$ nm. The hopping rate of singlet excitons between host molecules of TPD is $\nu_h = 6D_S/R_{XX}^2 \cong 2.5 \times 10^9$ s^{-1}. The energy transfer rate constant can be evaluated from the Förster radius $R_0 \cong 3$ nm, intrinsic exciton lifetime, $\tau_S = 1$ ns (Ref. 34) and R_{XY} as $k_{XY}^{(S)} = \tau_S^{-1}(R_0/R_{XY})^6 \cong 2 \times 10^{12}$ s^{-1} (see Ref. 26). Thus, $\nu_h/k_{XY}^{(S)} \cong 1.25 \times 10^{-3}$ which reflects well the relation $\gamma_{Sq}(X+Y)/\gamma_{Sq}(X) = D_S(X+Y)/D_S(X) \cong (3 \cdot 10^{-5}$ cm^2/s)/(5×10^{-3} cm^2/s) $\cong 0.6 \times 10^{-2}$ between singlet exciton annihilation rate constants in blend $(X+Y)$ and neat TPD (X) films. Comparing τ_S with $[k_{XY}^{(S)}]^{-1}$ provides an evidence for the relation $k_{XY}^{(S)} \gg k_X$ assumed in solving the set of kinetics equations (4)–(7). The negligence of D_q might not be correct for Ir(ppy)$_3$ dispersed in high carrier mobility matrices such as TPD. For example, the time-of-flight measured electron and hole mobilities in similar films of $[4,4'$-N,N$'$-dicarbazole-diphenyl (CBP):Ir(ppy)$_3$8 wt. %], has been found to follow a typical Poole-Frenkel type field increase (see Sec. III B) with a scaling factor $\beta_\mu \approx 10^{-3}$ (cm/V)$^{1/2}$.[35] This yields $D_q \approx 10^{-9}$–10^{-8} cm^2/s at fields above 0.8 MV/cm, the values much less than D_S, but comparable with D_T at room temperature. Thus, one would expect a field increase in γ_{Tq} which in the case of Ir(ppy)$_3$ triplets shows up in a noticeable deviation of $\delta_q^{(T)}(F)$ data from its linear approximation in Fig. 7(a). However, the difference between the zero field and a high field value of the triplet-charge carrier interaction rate constant $|\gamma_{Tq}(F=0) - \gamma_{Tq}(F=10^6 \text{ V/cm})| \approx 1.5 \times 10^{-14}$ cm^3/s, due to this deflection, does not exceed a factor of 1.5 of its average value resulting from the slope of the straight-line plot of $\delta_q^{(T)}(F)$ as demonstrated above.

D. Dissociation versus charge quenching

Recalling the results of the preceding section, it is seen that the presence of holes injected from the ITO anode into the emitter bulk reduces excitons' lifetime leading to PL quenching effects. The quantitative data have been based on the premise that the quenching observed in the Al/emitter/Al structure is due solely to exciton dissociation. However, exciton-charge carrier interaction is conceivable to occur in this structure due to charge carriers (electrons) injected possibly at the Al electrode/emitter interface. This point is of crucial importance for the separation of field- and charge-induced PL quenching mechanisms. To assess the role of the charge injected on Al contacts, an asymmetry in the dark current for positive (j^+) and negative (j^-) polarization of top electrode Al [Fig. 8(b)] could be employed and a difference or its lack in the dc EML effect observed. However, due to low signals and the long retention time of the charge in samples, highly unreliable (irreproducible) results are ob-
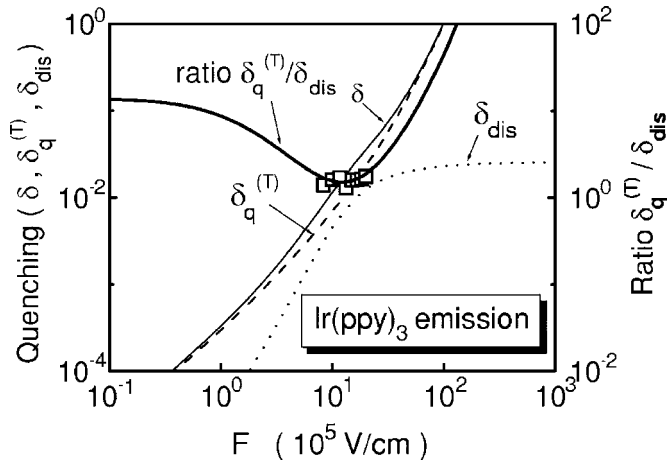
FIG. 10. Comparison of the total (δ), charge-induced (δ_q), and dissociation (δ_{dis}) component electric field evolution of the phosphorescence quenching along with the field dependence of the δ_q/δ_{dis} ratio. The solid curves represent theoretical plots according to Eq. (14) for δ_{dis} (using Onsager parameters $\eta_0 = 0.025$ and $r_0/r_c = 0.115$), according to Eq. (18) for δ_q (using $\varepsilon = 3$, $\tau_T = 1.5$ μs, and $\gamma_0 = 8 \times 10^{-15}$ cm^3/s), and according to Eq. (18) for δ_q/δ_{dis} with parameters as above. The overall quenching effect δ is obtained by summing these two components. The squares stand for the δ_q/δ_{dis} ratio resulting from the experiment.

tained using the steady-state electric field modulation method. A plausible alternative was to use a phase sensitive technique applying alternating voltage [Fig. 1(a)] and recording the second harmonic PL signal (1). By this a possibility to reproducibly measure low signals has been accomplished and, moreover, the elimination of the PL quenching by deeply trapped charge achieved. With the alternating voltage frequency $\nu \approx 200$ Hz–2 kHz, only the exciton-free charge carrier quenching could eventually be detected in the modulation signal. The measured second harmonic PL quenching signals showed no dependence on ν within this range and, moreover, its phase shift with respect to the fundamental frequency of the ac applied voltage was observed. The presence of the trapped charge has been detected by the independent electroabsorption measurements at first and second harmonics as described in Ref. 19. For the thermal release times $\tau_{rel} > \nu^{-1} \sim 5$ ms (average trap depth ≈ 0.5 eV), the trapped carriers do not contribute to the ac modulation effect. On the other hand, the concentration of free charges ($n_e \approx 4 \times 10^{11}$/cm^3 at F=10^6 V/cm), calculated from the highest steady-state current [see Fig. 8(b)] with the high-field mobility $\mu(F=10^6$ V/cm$) \approx 1.5 \times 10^{-7}$ cm^2/V s,[35] is too low to modulate the PL signal on the 0.1% level with any realistic value of the interaction rate constant. For example, taking $\delta_S \approx 0.2\%$ at $F=10^6$ V/cm for the fluorescence of TPD component in Fig. 5, we find $\gamma_{Sq} \approx \delta_S/n_e\tau_S \approx 5 \times 10^{-6}$ cm^3/s [$\tau_S = 1$ ns (Ref. 34)] which, in turn, yields the singlet exciton diffusion coefficient $D_S \approx 4$ cm^2/s, the value that unrealistically exceeds by three orders of magnitude the value of D_S for 100% TPD layer.[34] Therefore, the only reason for the ac PL quenching in samples with Al/Al electrodes is the electric field-assisted dissociation of the emissive states. In contrast, the much higher EML effect for the ITO(+)/emitter/
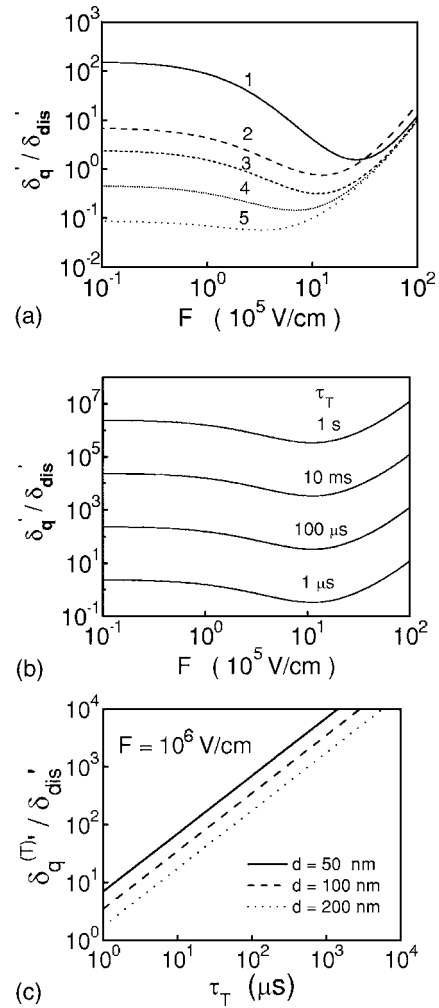

FIG. 11. The theoretical predictions according to Eq. (18) of the charge-induced component relative to dissociation-imposed quenching (δ_q'/δ_{dis}') as a function of electric field and exciton lifetime (τ_T). The curves are parametric in r_0/r_c (1: 0.08, 2: 0.10, 3: 0.12, 4: 0.15; 5: 0.20) with $\eta_0 = 0.1$ for a sample $d = 100$ nm and $\tau = 1$ μs (a); τ_T with $\eta_0 = 0.1$, $r_0/r_c = 0.12$, and $d = 100$ nm, $\gamma_0 = 8 \times 10^{-15}$ cm^3/s, and $\beta_q = 1.3 \times 10^{-3}$ (cm/V)$^{1/2}$ (b); and $d = 50–200$ nm with $\eta_0 = 0.1$, $r_0/r_c = 0.12$, and $\delta_{dis} = 2.15\%$ (c).

Au($-$) structure allowed us to apply successfully the dc modulation technique as sketched in Fig. 1(b) and illustrated in Fig. 3. The hole injection current in this structure exceeds 3 to 4 orders of magnitude the electron injection in the Al/emitter/Al structure (see Fig. 8), which along with its SCL behavior (3) indicates a fast release of shallow trapped holes. Consequently, a 10 s duration field step resulted in the charge concentration change given by $\bar{n}$ (15).

We now compare the PH quenching imposed by dissociation (δ_{dis}) of unrelaxed triplet excited states and that resulted from relaxed triplet exciton-charge carrier interaction [$\delta_q^{(T)}$]. In Fig. 10 both $\delta_q^{(T)}$ and δ_{dis} along with their ratio [$\delta_q^{(T)}/\delta_{dis}$] and total quenching signal, $\delta = \delta_{dis} + \delta_q^{(T)}$, are presented as a function of electric field. It follows from the models described in Secs. IV B and IV C that the charge quenching $\delta_q^{(T)}$ increases linearly or slightly supralinearly with electric field (assuming ohmicity of the injecting contacts to be preserved)

whereas the initially increasing dissociation component of the quenching (δ_{dis}) saturates at high electric fields ($F > 10^6$ V/cm). This leads their ratio

$$\frac{\delta_q^{(T)}}{\delta_{dis}} = \frac{3}{2} \frac{e\varepsilon_0\varepsilon\tau_T\gamma_{Tq}r_0 F^2}{kTd\eta_0\left[1 - (eFr_0/kT)\sum_{m=1}^{\infty} P_m(r_c/r_0)P_m(eFr_0/kT)\right]}$$

(18)

to reveal a minimum at a field F_{min} dependent on characteristic parameters of two coexisting mechanisms of exciton quenching. An obvious message that follows from this non-monotonic behavior of the δ_q-to-δ_{dis} ratio is that increasing field reduces progressively the role of the charge quenching mechanism of PL in the low field limit in favor of the dissociation quenching which becomes less important at high electric fields. To improve performance of organic LEDs the contribution of component δ_q must be minimized using materials with strongly bound excitons and strong off-diagonal disorder. The former translates into a weak dissociation ability of excited states, reflected in low values of Onsager parameters η_0 and r_0.

To illustrate how the field-dependent relative contributions of two quenching components (δ_{dis}, δ_q) respond to various model parameters, plots $\delta_q'^{(T)}/\delta_{dis}$ as a function of F are presented in Fig. 11 for a slightly increasing function of $\gamma_{Tq}(F) = \gamma_0 \exp(\beta_q F^{1/2})$ with $\gamma_0 = 8 \times 10^{-15}$ cm³/s and $\beta_\mu = 1.3 \times 10^{-3}$ (cm/V)$^{1/2}$, typical emitter thicknesses $d = 50-200$ nm and variable exciton lifetime, τ_T. They demonstrate that the minimum of the ratio $\delta_q'^{(T)}/\delta_{dis}$ occurs at F_{min} well above 10^5 V/cm and shifts still towards higher fields by about one order of magnitude as the initial separation parameter, r_0, decreases from 3.8 to 1.5 nm [Fig. 11(a)]. We note that according to Eq. (18) varying the initial dissociation efficiency, η_0, does not change the minimum position, but shifts the curve up or down (not shown in the figure). Following the predictions of Eq. (18), a monotonous shift to higher values of the ratio is observed as the triplet lifetime increases [Fig. 11(b)] and sample thickness decreases [Fig. 11(c)].

V. CONCLUSIONS

The quantum efficiency roll-off observed commonly with organic LEDs operating at high electric fields is due to in-creasing fate of emissive states and their precursors. Studying the PL emission from typical phosphorescent LED emitters such as Ir(ppy)$_3$ in electric fields at relatively low light excitation intensities we demonstrated the PL quenching to be in general underlain by the coexistence of two mechanisms: (i) electric-field assisted dissociation, and (ii) exciton-charge carrier interaction. They could be separated and their contributions to the total quenching effect (δ) established by an examination of identical systems provided with a combination of either low- or high-work function electrical contacts. A demarcation electric field strength (F_{min}) can be defined, where the dissociation quenching component (δ_{dis}), following the 3D Onsager model of geminate recombination, saturates but charge quenching component (δ_q) still increases monotonously. The ratio δ_q / δ_{dis} reveals a minimum at that field, the charge quenching component becomes maximally reduced. The F_{min} is linked to the likelihood of geminate recombination of charge pairs created from excitons. Efforts to reduce the electric field quenching effect should therefore concentrate on minimizing the initial dissociation efficiency and separation distance between pair carriers produced in the course of exciton dissociation that is to select emitters with strongly bound excitons. The charge quenching component has been shown to occur through either mobile exciton-charge carrier interaction governed by exciton diffusion and a charge carrier motion-affected process for slow (or immobile) excitons. Its reduction requires molecular systems with low exciton diffusivity and relatively strong disorder in addition to short lifetime of triplet excitons. Manipulating sample parameters such as thickness or ambient conditions such as temperature allows us to optimize the charge-to-dissociation quenching ratio.

Once both the origin of the quenching of excited states and electrical processes are quantified, methods for molecular scale and device structures manipulation for the prediction of the emission efficiency of organic emitters at high electric fields may become possible.

[1] J. Kalinowski, *Organic Light Emitting Diodes: Principles, Characteristics, and Processes* (Marcel Dekker, New York, 2005).

[2] M. A. Baldo, D. F. O'Brien, Y. You, A. Shoustikov, S. Sibley, M. E. Thompson, and S. R. Forrest, Nature (London) **395**, 151 (1998).

[3] C. Schmitz, M. Thelakkat, and H. W. Schmidt, Adv. Mater. (Weinheim, Ger.) **11**, 821 (1999).

[4] M. A. Baldo, M. E. Thompson, and S. R. Forrest, Nature (London) **403**, 750 (2000).

[5] M. A. Baldo, C. Adachi, and S. R. Forrest, Phys. Rev. B **62**, 10967 (2000).

[6] J. Kalinowski, W. Stampor, J. Mężyk, M. Cocchi, D. Virgili, V. Fattori, and P. Di Marco, Phys. Rev. B **66**, 235321 (2002).

[7] J. Kalinowski, L. C. Palilis, W. H. Kim, and Z. H. Kafafi, J. Appl. Phys. **94**, 7764 (2003).

[8] M. Cocchi, V. Fattori, D. Virgili, C. Sabatini, P. Di Marco, M.

Maestri, and J. Kalinowski, Appl. Phys. Lett. **84**, 1052 (2004).

[9] J. Kalinowski, W. Stampor, M. Cocchi, D. Virgili, and V. Fattori, Appl. Phys. Lett. **86**, 241106 (2005).

[10] J. Mężyk, J. Kalinowski, F. Meinardi, and R. Tubino, Chem. Phys. Lett. **395**, 321 (2004).

[11] C. Adachi, M. A. Baldo, and S. R. Forrest, J. Appl. Phys. **87**, 8049 (2000).

[12] J. Mężyk, J. Kalinowski, F. Meinardi, and R. Tubino, Appl. Phys. Lett. **86**, 111976 (2005).

[13] J. Kalinowski, J. Mężyk, F. Meinardi, R. Tubino, M. Cocchi, and D. Virgili, J. Appl. Phys. **98**, 063532 (2005).

[14] J. Kalinowski, M. Cocchi, G. Giro, V. Fattori, and P. Di Marco, J. Phys. D **34**, 2282 (2001).

[15] L. Onsager, Phys. Rev. **54**, 554 (1938).

[16] J. Szmytkowski, W. Stampor, J. Kalinowski, and Z. H. Kafafi, Appl. Phys. Lett. **80**, 1465 (2002).

[17] J. Kalinowski, J. Phys. D **32**, R179 (1999).

[18] J. Kalinowski, W. Stampor, and P. Di Marco, J. Chem. Phys. **96**, 4136 (1992).

[19] W. Stampor, J. Kalinowski, and P. Di Marco, Mol. Cryst. Liq. Cryst. **228**, 233 (1993).

[20] P. N. Murgatroyd, J. Phys. D **3**, 151 (1970).

[21] G. G. Malliaras and J. C. Scott, J. Appl. Phys. **85**, 7426 (1999).

[22] M. Stolka, J. F. Janus, and D. M. Pai, J. Phys. Chem. **88**, 4707 (1984).

[23] Y. Shen, M. W. Klein, D. B. Jacobs, J. C. Scott, and G. G. Malliaras, Phys. Rev. Lett. **86**, 3867 (2001).

[24] L. Firley and A. Zahab, in *Book of Abstracts of the NATO ARW ERPOS-7 Conference* (ISSN 1426-36-96, Wrocław 1996), p. 85.

[25] C. A. Hogarth, Proc. SPIE **2780**, 25 (1996).

[26] J. Kalinowski, W. Stampor, M. Cocchi, D. Virgili, V. Fattori, and P. Di Marco, Chem. Phys. **297**, 39 (2004).

[27] M. I. Khan, G. C. Bazan, and Z. D. Popovic, Chem. Phys. Lett. **298**, 309 (1998).

[28] A. Nollau, M. Hoffmann, T. Fritz, and K. Leo, Thin Solid Films **368**, 130 (2000).

[29] Z. D. Popovic, M. I. Khan, A. M. Hor, J. L. Goodman, and J. F. Graham, J. Phys. Chem. B **106**, 8625 (2002).

[30] M. Tachiya, J. Chem. Phys. **69**, 2375 (1978).

[31] M. Wojcik and M. Tachiya, Radiat. Phys. Chem. **74**, 132 (2005).

[32] M. Tachiya, J. Chem. Phys. **89**, 6929 (1988).

[33] W. Helfrich, in *Physics and Chemistry of Organic Solid State*, edited by D. Fox, M. M. Labes, and A. Weissberger (Intersci. Publ., New York, 1967), Vol. III, Chap. 1.

[34] J. Kalinowski, G. Giro, P. Di Marco, N. Camaioni, and V. Fattori, Chem. Phys. Lett. **265**, 607 (1997).

[35] S.-B. Lee, T. Yasuda, M.-J. Yang, K. Fujita, and T. Tsutsui, Mol. Cryst. Liq. Cryst. **405**, 67 (2003).